J. Fluid Mech. (2006), *vol.* 554, *pp.* 411–431.
doi:10.1017/S002211200600886X Printed in the United Kingdom

The effects of solid boundaries on confined two-dimensional turbulence

By G. J. F. VAN HEIJST, H. J. H. CLERCX AND D. MOLENAAR

Fluid Dynamics Laboratory, Department of Physics, Eindhoven University of Technology, P.O. Box 513, NL-5600 MB Eindhoven, The Netherlands

(Received 8 March 2005 and in revised form 16 December 2005)

This paper addresses the effects of solid boundaries on the evolution of two-dimensional turbulence in a finite square domain, for the cases of both decaying and continuously forced flow. Laboratory experiments and numerical flow simulations have revealed the crucial role of the solid no-slip walls as sources of vorticity filaments, which may significantly affect the flow evolution in the interior. In addition, the walls generally provide normal and tangential stresses that may exert a net torque on the fluid, which can change the total angular momentum of the contained fluid. For the case of decaying turbulence this is observed in so-called 'spontaneous spin-up', i.e. a significant increase of the total angular momentum, corresponding to a large domain-filling circulation cell in the organized 'final' state. For the case of moderate forcing this phenomenon may still be observed, although the filamentary vortex structures advected away from the walls may cause erosion and possibly a total destruction of the central cell. This disordered stage – characterized by a significantly decreased total angular momentum – is usually followed by a re-organization into a large circulation cell (in either the same or opposite direction) with an increased total angular momentum. The scaling behaviour of vorticity structure functions and the probability distribution function of vorticity increments have been investigated for forced turbulence and indicate a strong anisotropy of the turbulent flow in the range of Reynolds numbers considered.

1. Introduction

Two-dimensional turbulent flows are characterized by the inverse energy cascade, i.e. by a spectral flux of kinetic energy to smaller wavenumbers. This applies in particular to the case of statistically steady forced flow, in which the overall kinetic energy input is in balance with the energy dissipation at the smallest scales of the flow. In the case of decaying turbulence – in which the flow is initialized at $t = 0$ and subsequently allowed to evolve – the so-called selective decay mechanism also plays an essential role, according to which the flow structures at smaller length scales decay faster than those at larger scales (see Matthaeus & Montgomery 1980). In fact, this mechanism then competes with the inverse energy cascade. In either case, the flow has a tendency to form larger, coherent vortex structures. This behaviour was shown for the case of decaying turbulence in numerical simulations by Matthaeus & Montgomery (1980), McWilliams (1984), and Santangelo, Benzi & Legras (1989). For an overview of the theory of two-dimensional turbulence we refer to Kraichnan & Montgomery (1980), and for some recent experiments the reviews by Tabeling

(2002) and Kellay & Goldburg (2002) can be consulted. Most of the experiments discussed in these reviews disregard the role of (no-slip) boundaries. The present paper addresses the effect of no-slip boundaries on the evolution of two-dimensional turbulence.

In a numerical simulation of decaying two-dimensional turbulence on a bounded, circular domain Li & Montgomery (1996) and Li, Montgomery & Jones (1996, 1997) observed flow behaviour that is completely different from that on a double-periodic domain; details of the flow evolution were found to depend to some degree on the type of boundary conditions applied, i.e. stress-free or no-slip. Experiments on decaying turbulence in linearly stratified and in two-layer fluids in circular containers by Maassen, Clercx & van Heijst (1999, 2002) confirmed the decay process as reported by Li *et al.* (1997).

In their numerical study of decaying turbulence in a square domain with solid walls, Clercx *et al.* (1999) found similar effects of the boundaries. In particular for the case of no-slip boundary conditions, the walls play an active role in the flow evolution, namely as sources of filaments of high-amplitude vorticity. Whenever a (small-scale) vortex structure approaches a solid no-slip wall, a boundary layer is formed that contains opposite-signed vorticity. This boundary layer is partially 'scraped off' from the wall in the form of a long vorticity filament that may be wrapped around the vortex or otherwise be advected into the interior of the flow domain. This process of vorticity filament production at the no-slip walls continues even during the later stages of the flow evolution when the domain is filled with large-scale vortices. It also has a significant effect on the spectral characteristics of the turbulence, as was revealed in a numerical study by Clercx & van Heijst (2000).

While decaying turbulence on a double-periodic square domain eventually becomes organized in the form of a combination of two cells of positive and negative circulations (see Matthaeus *et al.* 1991), the 'final state' of decaying turbulence in a square domain with no-slip boundaries consists of a single large central cell with either positive or negative circulation, surrounded by a shielding ring of opposite vorticity (such that the total circulation of the flow is zero, as dictated by the no-slip boundary condition). This long-time behaviour has been observed both in laboratory experiments (Maassen *et al.* 2002) and in high-Reynolds-number simulations of decaying two-dimensional turbulence (Clercx *et al.* 2001).

A remarkable observation was that in many cases the total angular momentum $L(t)$ of the flow (being randomly initialized, with $L(t=0) \simeq 0$) shows a sudden change to non-zero values – a feature termed 'spontaneous spin-up'. This spin-up of the fluid is directly associated with the self-organization of the flow into a single larger vortex structure (see Clercx, Maassen & van Heijst 1998; Clercx *et al.* 2001). In the next stage of the flow evolution, the absolute angular momentum $|L(t)|$ shows a very slow decay to zero for very late times. It is important to note that the no-slip boundary condition is a prerequisite for the spin-up, as the angular momentum $L(t)$ is an irrelevant quantity for the flow evolution on a double-periodic domain. Also, the square domain geometry is important, spin-up being virtually absent on a circular domain or on a long rectangular domain in which the 'final state' consists of a linear (domain-filling) array of counter-rotating cells, see Maassen, Clercx & van Heijst (2003). Obviously, the change of the total angular momentum during the spontaneous spin-up is connected with the action of forces at the domain boundaries. Numerical simulations have revealed that – for the case of a square geometry – the contribution of the inviscid normal stress (i.e. the pressure) is much larger than the effects of viscous shear and normal stresses.

In recent direct numerical simulations of stochastically forced two-dimensional turbulent flow in a square domain with no-slip boundary conditions we also observed spontaneous spin-up behaviour, although remarkably different from the decaying case. In the forced turbulence simulations one observes several consecutive events of rapid increase and decrease of $|L(t)|$, often with sign reversal of $L(t)$ between neighbouring peaks in $|L(t)|$.

Obviously, the presence of no-slip boundaries has a significant effect on the evolution of bounded two-dimensional turbulence, both for the decaying and the continuously forced case. In this paper we will address some of the crucial features of these wall effects. The role of boundary conditions in integral quantities like total circulation, angular momentum, kinetic energy and enstrophy will be discussed in § 2. Some experimental and numerical results on decaying turbulence on a square domain with no-slip walls will be reviewed in § 3, while § 4 presents some recent numerical simulation results obtained for the case of a continuous time-dependent forcing. For the latter case, the behaviour of the total angular momentum during the flow evolution and the scaling behaviour of the flow will be discussed. Some general conclusions will be drawn in § 5.

2. Some notes on boundary conditions and integral quantities

The two-dimensional motion of an incompressible, viscous fluid on a bounded domain $\mathscr{D}$ is conveniently described in a Cartesian frame of reference $\boldsymbol{x} = (x, y, z)$, with (x, y) the coordinates in the plane of the flow. The (horizontal) flow field is then given by $\boldsymbol{v} = (u, v, 0)$ and the vorticity by $\boldsymbol{\omega} = \nabla \times \boldsymbol{v} = (0, 0, \omega)$, with $\omega = \partial v/\partial x - \partial u/\partial y$ the component in the (vertical) z-direction. For the case of a Newtonian fluid, the motion is governed by the Navier–Stokes equation, which is in non-dimensional form

$$\frac{\partial \boldsymbol{v}}{\partial t} + (\boldsymbol{v} \cdot \nabla)\boldsymbol{v} = -\nabla p + \frac{1}{Re}\nabla^2 \boldsymbol{v} + \boldsymbol{f} \tag{2.1}$$

with t the time, p the pressure and $Re = VL/\nu$ the Reynolds number based on characteristic velocity and length scales V and L, respectively, ν the kinematic viscosity and $\boldsymbol{f}(\boldsymbol{x}, t)$ an external forcing. Alternatively, one may describe the flow by the vorticity equation, which is obtained by taking the curl of (2.1):

$$\frac{\partial \omega}{\partial t} + (\boldsymbol{v} \cdot \nabla)\omega = \frac{1}{Re}\nabla^2 \omega + q, \tag{2.2}$$

where $q(\boldsymbol{x}, t) = (\nabla \times \boldsymbol{f}) \cdot \hat{\boldsymbol{k}}$, with $\hat{\boldsymbol{k}}$ the unit vector in z-direction.

Solutions of either equation have to satisfy conditions imposed by the domain boundary $\partial\mathscr{D}$. Impermeability of this boundary implies that the normal velocity component should vanish, i.e.

$$\boldsymbol{v} \cdot \hat{\boldsymbol{n}} = 0 \quad \text{on} \quad \partial\mathscr{D}, \tag{2.3}$$

with $\hat{\boldsymbol{n}}$ the unit (outward) normal on the boundary. After introduction of the stream function Ψ by $\boldsymbol{v} = \nabla \times \hat{\boldsymbol{k}}\Psi$, this boundary condition can also be written as $\Psi = \text{constant}$ on $\partial\mathscr{D}$. In the case of a physically realistic wall, the flow has to satisfy the no-slip condition $v_{\|} = 0$ on $\partial\mathscr{D}$, with $v_{\|}$ the tangential velocity component. Combination of the no-slip and impermeability conditions leads to

$$\boldsymbol{v} = \boldsymbol{0} \quad \text{on} \quad \partial\mathscr{D}. \tag{2.4}$$

Any solution of (2.1) for a viscous flow on a domain bounded by a physical wall has to satisfy this condition (2.4). A description of the flow as a solution of the vorticity equation (2.2) requires the value of ω on the domain boundary, but this value is not provided *a priori*.† In numerical flow simulations based on the time-discretized version of (2.2), the boundary value of ω is determined by using an influence matrix method (for details, see Clercx 1997).

The strict no-slip boundary condition can be relaxed to some extent by considering a stress-free boundary, which implies

$$(\hat{\boldsymbol{n}} \cdot \boldsymbol{\tau})_{\|} = 0 \quad \text{on} \quad \partial\mathscr{D}, \tag{2.5}$$

with $\boldsymbol{\tau}$ the viscous stress tensor (note that the stress-free boundary condition is not equivalent to a free-slip boundary condition for inviscid flows). For the particular case of a square or rectangular domain, combination of the latter condition and the impermeability condition (2.3) leads to

$$\omega = 0 \quad \text{on} \quad \partial\mathscr{D}. \tag{2.6}$$

Imposing a periodic boundary condition for the flow in such a square domain, given by $\{-1 \leqslant x \leqslant 1, -1 \leqslant y \leqslant 1\}$, would imply

$$\boldsymbol{v}(-1, y) = \boldsymbol{v}(1, y), \boldsymbol{v}(x, -1) = \boldsymbol{v}(x, 1), \tag{2.7}$$

while the vorticity ω can take any value on $\partial\mathscr{D}$, provided the periodicity condition is satisfied.

In order to understand the global behaviour of the confined flow, it is useful to describe the flow in terms of integral quantities. The total circulation Γ of the flow is defined as

$$\Gamma = \oint_{\partial\mathscr{D}} \boldsymbol{v}(\boldsymbol{r}, t) \cdot \mathrm{d}\boldsymbol{s} = \int_{\mathscr{D}} \omega \, \mathrm{d}A \tag{2.8}$$

with $\boldsymbol{r} = (x, y)$ the position vector and $\mathrm{d}\boldsymbol{s}$ an infinitesimal element of the boundary $\partial\mathscr{D}$. It is straightforward to verify that $\Gamma = 0$ for both double-periodic boundaries and no-slip boundaries; in contrast, the value of Γ is not determined for the flow confined by a stress-free boundary. An expression for the rate of change of Γ can be derived by integrating the vorticity equation (2.2) term by term over the whole domain $\mathscr{D}$. After applying either the no-slip or the stress-free boundary conditions (2.4) and (2.6), respectively, one arrives at

$$\frac{\mathrm{d}\Gamma}{\mathrm{d}t} = \frac{1}{Re} \oint_{\partial\mathscr{D}} \hat{\boldsymbol{n}} \cdot \nabla\omega \, \mathrm{d}s + \int_{\mathscr{D}} q \, \mathrm{d}A. \tag{2.9}$$

This result states that the total circulation of freely evolving (i.e. unforced, $q = 0$) flow on a bounded domain $\mathscr{D}$ can only change through a net vorticity flux associated with diffusion through the boundary $\partial\mathscr{D}$. For the double-periodic and no-slip boundary cases, $\Gamma = 0$ implies that $\mathrm{d}\Gamma/\mathrm{d}t = 0$, i.e. zero net leakage of vorticity through $\partial\mathscr{D}$. Only in the case of a stress-free boundary may the diffusive vorticity flux through the boundary (and in the case of forced flow: a non-zero forcing $\int_{\mathscr{D}} q \mathrm{d}A$) result in a change in the total circulation Γ. In summary, for the various types of boundary

† A similar problem exists for solution of the Navier–Stokes equation (2.1), where the boundary value for the pressure is not provided *a priori*.

conditions the total circulation has the following properties:

$$\text{double-periodic domain:} \quad \Gamma = 0, \quad \frac{\mathrm{d}\Gamma}{\mathrm{d}t} = 0;$$

$$\text{no-slip boundaries:} \quad \Gamma = 0, \quad \frac{\mathrm{d}\Gamma}{\mathrm{d}t} = 0;$$

$$\text{stress-free boundaries:} \quad \Gamma \quad \text{and} \quad \frac{\mathrm{d}\Gamma}{\mathrm{d}t}: \quad \text{no specified value.}$$

The quasi-stationary late-time states of confined two-dimensional flows have been analysed by a statistical mechanical approach, based on a system of point vortices for which a maximum entropy solution was sought (Onsager 1949; Joyce & Montgomery 1973). Later, an alternative approach was based on a patchwise discretization of the vorticity field (Miller 1990; Robert 1991). The predictions based on these (inviscid) statistical mechanical theories crucially depend on the conditions imposed at the boundaries of the domain, which were either double-periodicity or free-slip walls (bounded inviscid flows). Examples of the application of the statistical mechanical approach to inviscid flows in bounded square containers with free-slip walls were provided by Pointin & Lundgren (1976) for the point-vortex discretization and by Chavanis & Sommeria (1996) for the patchwise discretization of vorticity. Although in terms of the total circulation the no-slip condition seems equivalent to double-periodicity of the domain, the action of viscosity in such flows rules out any description by inviscid theories. A detailed discussion of this issue is given by Brands, Maassen & Clercx (1999).

Another relevant global quantity of the flow is its total angular momentum L, defined with respect to the origin in the domain centre as

$$L = \int_{\mathscr{D}} \hat{\boldsymbol{k}} \cdot (\boldsymbol{r} \times \boldsymbol{v}) \, \mathrm{d}A. \tag{2.10}$$

An expression for its rate of change is derived by taking the time derivative and inserting the Navier–Stokes equation (2.1) in the integral. For a flow on a domain enclosed by an impermeable boundary (on which condition (2.3) applies) one thus obtains

$$\frac{\mathrm{d}L}{\mathrm{d}t} = \oint_{\partial\mathscr{D}} p\boldsymbol{r} \cdot \mathrm{d}\boldsymbol{s} + \frac{1}{Re} \oint_{\partial\mathscr{D}} \omega(\boldsymbol{r} \cdot \hat{\boldsymbol{n}}) \, \mathrm{d}s - \frac{2}{Re}\Gamma + M(t), \tag{2.11}$$

where

$$M(t) \equiv -\frac{1}{2} \int_{\mathscr{D}} r^2 q(\boldsymbol{r}, t) \, \mathrm{d}A \tag{2.12}$$

represents the net torque introduced by the forcing.

Obviously, in the unforced case ($M = 0$) the change in angular momentum is entirely due to the action of torques of boundary forces associated with the pressure (normal stress) and viscous stresses (normal and shear stress). Note that a circular domain forms a special case, because the torque of the normal wall stress is identically zero then.

Other global quantities that are useful in characterizing the flow are the total kinetic energy (per unit density)

$$E = \frac{1}{2}\int_{\mathscr{D}} |\boldsymbol{v}|^2 \,\mathrm{d}A = \frac{1}{2}\int_{\mathscr{D}} |\nabla\Psi|^2 \,\mathrm{d}A = \frac{1}{2}\int_{\mathscr{D}} \omega\Psi \,\mathrm{d}A \tag{2.13}$$

and the total enstrophy V, defined as

$$V = \frac{1}{2}\int_{\mathscr{D}} \omega^2 \,\mathrm{d}A. \tag{2.14}$$

For inviscid flows without forcing, equation (2.2) implies that vorticity is conserved, i.e. $\mathrm{D}\omega/\mathrm{D}t = 0$. It can be shown that this property in turn implies that both E and V are conserved as well. For viscous decaying flows the energy and enstrophy are no longer invariant, and their evolution is given by

$$\frac{\mathrm{d}E}{\mathrm{d}t} = -\frac{1}{Re}\int_{\mathscr{D}} \omega^2 \,\mathrm{d}A = -\frac{2}{Re}V(t), \tag{2.15}$$

$$\frac{\mathrm{d}V}{\mathrm{d}t} = -\frac{1}{Re}\int_{\mathscr{D}} |\nabla\omega|^2 \,\mathrm{d}A + \frac{1}{Re}\oint_{\partial\mathscr{D}} \omega(\hat{\boldsymbol{n}}\cdot\nabla\omega)\,\mathrm{d}s. \tag{2.16}$$

In the case of double-periodic or stress-free boundary conditions, the boundary integral in (2.16) is zero, and the enstrophy is apparently a monotonically decreasing function of time. In the limit of vanishing viscosity ($\nu \to 0$) this implies that $\lim_{\nu\to 0} \mathrm{d}E/\mathrm{d}t = 0$, i.e. the kinetic energy becomes a constant of motion.

For a flow bounded by no-slip walls, however, it is not clear *a priori* what value the boundary integral on the right-hand side of (2.16) reaches in this limit, so that a prediction of the time-behaviour of V is not possible.

To estimate the vorticity production at the no-slip boundaries a series of numerical experiments on a dipole collision with a no-slip wall has been conducted (with a high-resolution two-dimensional Chebyshev pseudo-spectral code, see Clercx 1997). The flow induced by the travelling dipole and the subsequent dipole–wall collision is not turbulent, but contains the essential ingredients needed to estimate the enstrophy production at the walls. A well-defined initial condition of the flow has been chosen, i.e. a condition satisfying zero velocity and vorticity at the domain boundaries at $t = 0$. In order to satisfy these constraints, a dipolar vortex structure, consisting of two equally strong, oppositely signed, isolated monopoles is released in the centre of the container and allowed to collide with the boundary at $t \approx 0.33$ (dimensionless time units). This set-up enables a systematic study of the Reynolds-number dependence of the vorticity production, and a number of normal and oblique dipole–wall collisions has been investigated numerically. This is illustrated here with an example of an oblique dipole–wall collision with $Re = 2500$ (based on the size and velocity of the initial dipole). Four snapshots of the dipole–wall collision are shown in figure 1, and in figure 2 we have plotted the vorticity and vorticity flux ($\partial\omega/\partial n$) profiles, respectively, at the boundary near the top right corner of the domain. High vorticity values at the boundary are found during the collision, in this particular case five times larger than the peak vorticity of the dipole itself, and the vorticity flux becomes extremely large after impact of the dipole on the no-slip wall (see, e.g., the data for $t = 0.6$). Many thin vorticity filaments and small-scale vortices have been produced. In

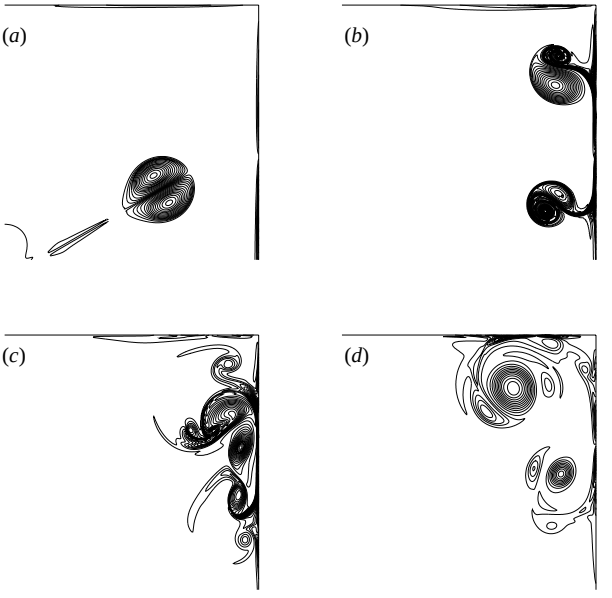

FIGURE 1. Vorticity contour plots of a simulation of an oblique dipole–wall collision with no-slip boundaries and $Re = 2500$. (*a*) $t = 0.2$, (*b*) $t = 0.4$, (*c*) $t = 0.6$, (*d*) $t = 1.0$. The vortex collision occurs at $t \approx 0.33$.

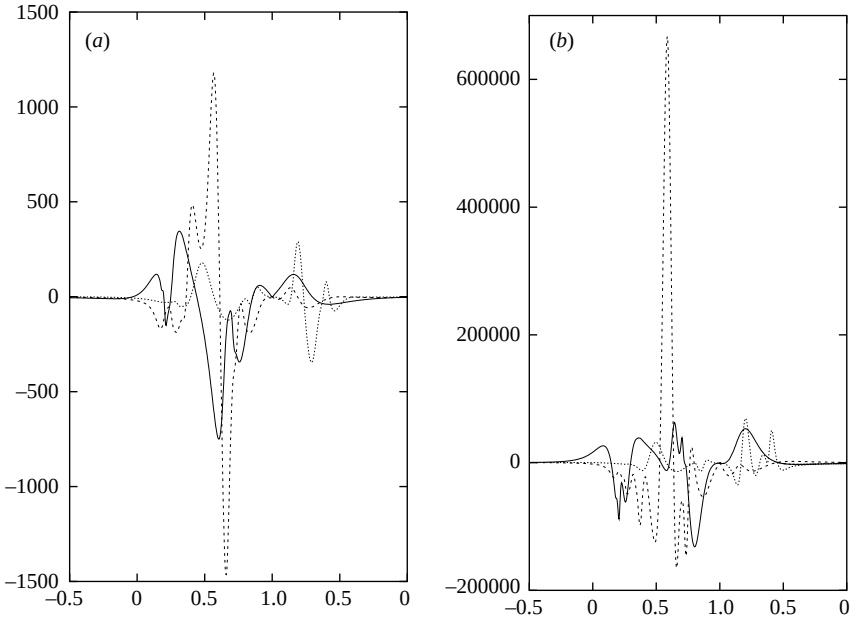

FIGURE 2. (*a*) Vorticity and (*b*) vorticity flux $\partial\omega/\partial n$ at the boundary $x = 1$ (with $-0.5 \leqslant y \leqslant 1$) and the boundary $y = 1$ (with $0 \leqslant x \leqslant 1$) for $t = 0.4$ (solid), $t = 0.6$ (dashed) and $t = 1.0$ (dotted) for the oblique dipole–wall collision experiment shown in figure 1 with $Re = 2500$.

order to resolve these small-scale structures, very high resolutions are needed during the simulations. In this particular case, with $Re = 2500$, a resolution of 385×385 Chebyshev polynomials is needed.

This run has been conducted for relatively low Reynolds number, but a series of Reynolds numbers has been considered (up to $Re = 1.6 \times 10^5$) to reveal the scaling of the enstrophy with the Reynolds number. It can be shown that the vorticity ω_{bl} contained in the thin boundary layers with thickness $\delta_{bl} \propto 1/\sqrt{Re}$ scales as $\omega_{bl} \propto \sqrt{Re}$, thus $V \propto \omega_{bl}^2 \delta_{bl} \propto \sqrt{Re}$. This scaling relation has been confirmed numerically (Clercx & van Heijst 2002). As a consequence, the dissipation of kinetic energy (see (2.15)) scales with $1/\sqrt{Re}$ instead of $1/Re$.

3. Decaying turbulence in a square no-slip domain

In this section we will briefly review the most noteworthy properties of decaying turbulent flow in a square domain with no-slip boundaries as observed in laboratory experiments and in numerical simulations.

3.1. *Experimental set-up*

The experiments were carried out in a square container of dimensions $100 \times 100 \times 30\,\mathrm{cm}^3$ (length $\times$ width $\times$ depth) which was filled with a two-layer salt stratification, consisting of a layer of fresh water on top of a layer of salty water, separated by an interfacial layer of typically a few centimetres depth.

Motion was generated by dragging a grid consisting of a linear array of vertical rods (3 mm diameter) horizontally through the fluid with a constant speed V. After having moved from one side to the opposite side of the tank, the grid was lifted out of the water. At large enough towing speed ($V \simeq 15\,\mathrm{cm\,s}^{-1}$) the motion in the wake of the grid is turbulent. In the homogeneous upper and lower layers, this motion is essentially three-dimensional and thus decays rapidly. The motion in the interfacial layer, however, is quasi-two-dimensional due to the action of the stratification: the flow field is planar, with considerable vertical gradients. The flow in the interfacial region was visualized by adding small neutrally buoyant polystyrene particles to the fluid. Illuminated by strip lights from the side, their motion was monitored by a CCD camera mounted above the container, and the data were stored on a computer. After each experiment the data were processed digitally, providing quantitative information about the flow field such as, e.g., the vorticity distribution.

Although strictly not two-dimensional, the planar motion in the interfacial region shows the phenomenological characteristics of two-dimensional turbulence, namely the emergence of larger, coherent vortex structures. This motion is very persistent, the decay mainly governed by vertical diffusion. A discussion of the dissipation of kinetic energy by vertical shearing (or vertical diffusion) in these experiments is given by Maassen *et al.* (2002), and the dissipation of kinetic energy agrees with previous observations obtained in experiments of freely decaying, stratified grid turbulence by Fincham, Maxworthy & Spedding (1996). In particular, it was found that horizontal dissipation accounts for less than 20 % of the total energy dissipation.

The effect of any initial angular momentum L_0 of the fluid on the subsequent flow evolution has been examined by using both symmetric and asymmetric grids. The initial angular momentum introduced during the forcing was controlled by changing the arrangement of the vertical rods in the rake. For the case of a not too closely packed rake, the drag force F_D of an individual rod can be estimated from $F_D = \frac{1}{2} C_D \rho V^2 l d$ with ρ the fluid density, l the rod length, and C_D the drag coefficient, for which empirical values for different Re-values can be found in Blevins (1984). Assuming that the (average) rod spacing is not too small, one may then estimate the

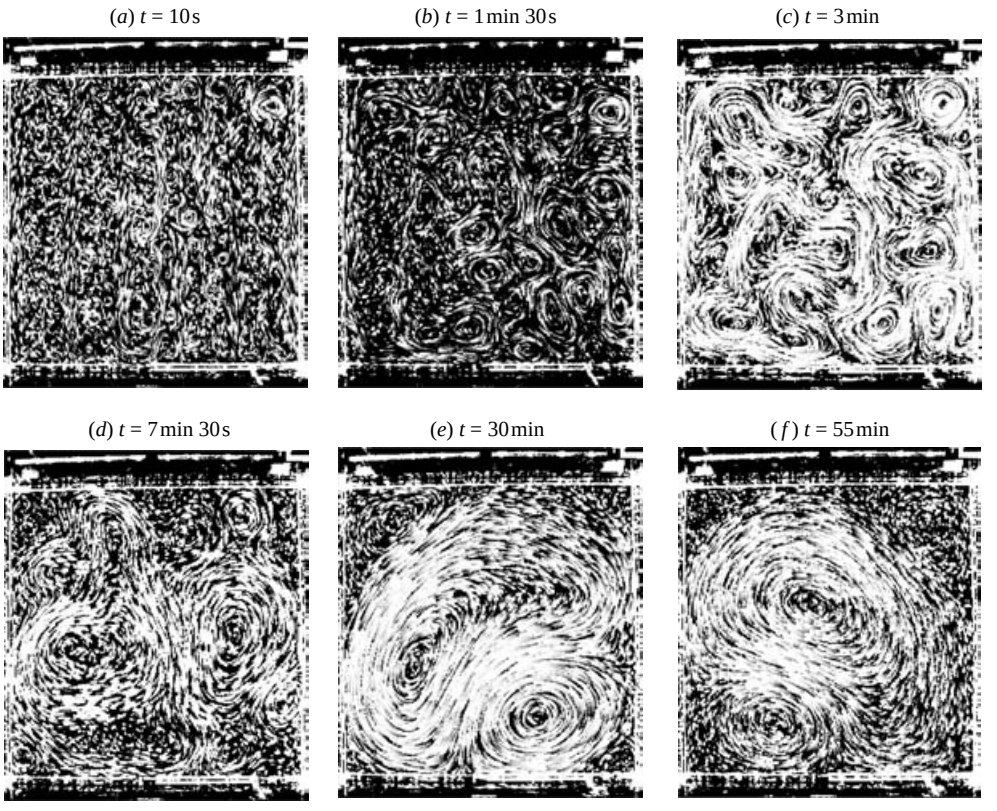

FIGURE 3. Sequence of streak images of a laboratory experiment in a square tank. The fluid motion was initialized by towing a rake horizontally through the fluid from one side to the opposite side. The images are taken from 10 s until 55 min after towing the rake through the fluid. The initial state (at $t = 10$ s) is characterized by $L_0 \approx 0$ and $Re^* \simeq 5000$. The tails of the streaks are generated after digital processing of the images (courtesy of Maassen 2000).

contribution of each rod in the rake to the total torque excerted on the fluid, and hence the total angular momentum introduced in the fluid during forcing.

The fluid motion generated by the grid forcing can be characterized by the Reynolds number based on the grid parameters: $Re_M = VM/\nu$, with M the average rod spacing. In the experiments discussed below, the parameter had typical values $V = 15\,\mathrm{cm\,s^{-1}}$ and $M = 4$ cm, yielding $Re_M \simeq 6000$. As an alternative, one can use the Reynolds number $Re^* = UW/\nu$ based on the half-width W of the tank and the root-mean-square velocity U of the initial flow field, as is usually done in numerical simulations. In the experiments U was measured typically 10 s after the grid forcing was stopped, yielding Re^*-values in the range 2000–5000. The decay rates of kinetic energy as measured in these laboratory experiments with $Re^* \approx 5000$ are of the same order as those computed in exactly two-dimensional flow simulations with $Re \approx 1500$–2000 (see Clercx *et al.* 1999). It appears that the two-dimensional simulations and the experiments can be compared directly for $Re \approx 0.4Re^*$.

3.2. *Observed flow evolution*

A typical sequence of streak images taken during an experiment with approximately zero initial angular momentum ($L_0 \approx 0$) is shown in figure 3. In the early stage of the flow evolution, the small-scale motions introduced by the moving grid are clearly

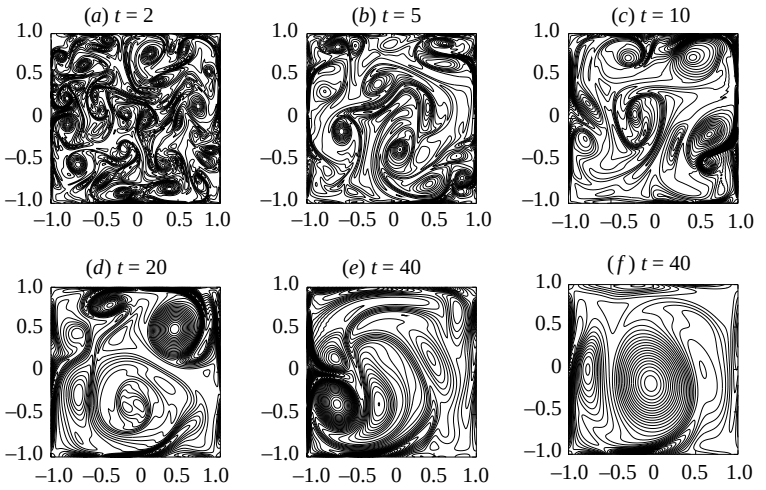

FIGURE 4. Sequence of vorticity contour plots for decaying two-dimensional turbulence in a square domain with no-slip boundaries according to a numerical simulation with a spectral code. The flow was initialized by a slightly disturbed array of 10×10 vortices with alternating sense of rotation, with $Re = 2000$. The contour level increment is: (*a*) 3, (*b*) 1.5, (*c*) 0.8, (*d*) 0.4, (*e*) 0.2, and (*f*) 0.1.

visible. It is also seen how the flow becomes gradually dominated by larger vortex structures. At a later stage (at $t = 55$ min) the flow consists of one large circulation cell and a small cell of opposite circulation. This double-cell structure was rather persistent, and continued to revolve until in the very late 'final' state it has changed into one single cell filling the domain completely. In addition to the vortex structures visible in the streak images, the vorticity contour plots obtained from these streak images (although not shown here, examples can be found in Maassen *et al.* 2002) reveal the existence of large gradients at the no-slip walls, in particular when vortices are approaching. One can also observe in these vorticity contour plots how vorticity filaments are peeled off from the walls, and then advected into the interior. These features can be distinguished better in the high-resolution simulation results presented in figure 4; the computations of this decaying flow were carried out with a spectral code developed by Clercx (1997), which can effectively deal with the large gradients in the flow field, in particular near the boundaries. In this numerical run the flow was initialized by a 10×10 array of Gaussian vortices of alternating polarity. In order to break any symmetry, the initial vortex positions and amplitudes were slightly perturbed in a random way.

In figure 5 we have plotted the enstrophy $V(t)$, the normalized enstrophy, $V(t)/E(t)$, and the palinstrophy

$$P(t) = \frac{1}{2} \int_{\mathscr{D}} |\nabla \omega|^2 \, \mathrm{d}A. \tag{3.1}$$

The palinstrophy is a measure of the vorticity gradients in the flow and represents an enstrophy sink (see (2.16)). We can conclude that the enstrophy shows similar power-law decay in each run irrespective of the perturbations of the initial array of 10×10 vortices, and the same conclusion can be drawn for the palinstrophy. The decay of the enstrophy from these numerical simulations compares remarkably well with the experimental data presented by Maassen *et al.* (2002): a power-law decay where

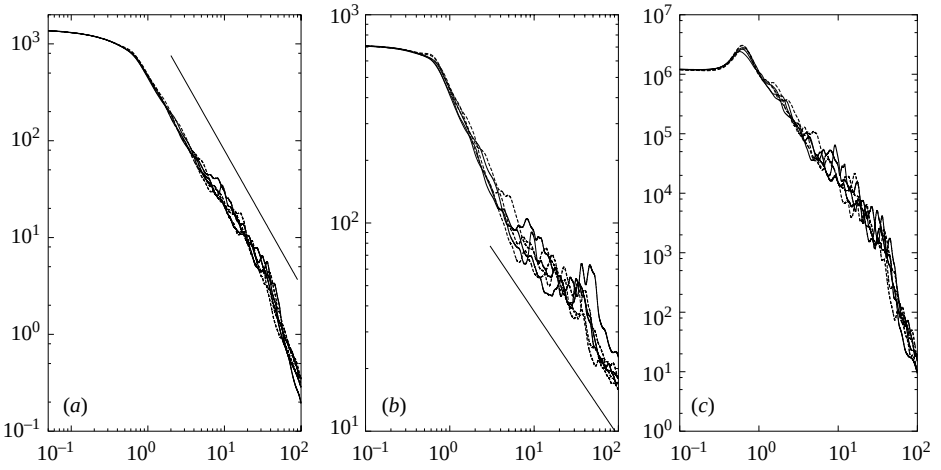

FIGURE 5. The decay of (*a*) the enstrophy, (*b*) the normalized enstrophy and (*c*) the palinstrophy of six runs with $Re = 2000$ are plotted as a function of the dimensionless time t. The lines in (*a*) and (*b*) represent power-law decay according to $t^{-1.4}$ and $t^{-0.6}$, respectively.

$V(t) \propto t^{-1.5}$ and a steeper decay at late times. The numerical data reveal $V(t) \propto t^{-1.4}$ and also a steeper decay at late times. A similar conclusion can be drawn for the normalized enstrophy: $V(t)/E(t) \propto t^{-0.5}$ in the experiment and $V(t)/E(t) \propto t^{-0.6}$ in the numerical simulations. It should, however, be noted that the experimental data for $V(t)/E(t)$ show more scatter.

The experiments and numerical results clearly reveal the active role of the no-slip boundaries as sources of large-amplitude vorticity filaments, even in the later stages of the flow evolution. It should be noted that the occurrence of vorticity filaments is not confined to regions close to the boundaries: as the vortex structures become larger and larger, the advection of wall vorticity takes place over larger distances, well into the interior of the flow domain. This behaviour is in sharp contrast with that observed on double-periodic domains, see e.g. McWilliams (1984) and Santangelo *et al.* (1989).

Both from the experimental and computed flow fields we determined the total angular momentum L of the fluid with respect to the tank centre, and a very similar behaviour was found: although the initial angular momentum was close to zero ($L_0 \approx 0$), in almost all runs it was observed that $L(t)$ quickly increased to a definite value, after which it decreased rather slowly. This 'spontaneous spin-up' of the flow is clearly seen in figure 6(*a*), which presents experimental results of the time evolution of the normalized angular momentum $L(t)/L_{sb}(t)$, with L_{sb} being the net angular momentum of the same fluid in a rigid-body rotation with the same kinetic energy $E(t)$ at that instant. A similar change in the total angular momentum was observed in runs with a randomly distributed initial vorticity, see e.g. Maassen *et al.* (2002), and the present numerical simulations with a totally different initial vorticity field i.e. the 10×10 array of Gaussian vortices, show similar spontaneous spin-up (see figure 6(*b*, *c*) for $L(t)$ and $L(t)/L_{sb}(t)$, respectively, for six different runs). This increase of $|L(t)|$ is associated with the formation of the larger circulation cell in or near the centre of the domain. As discussed in § 2, a net change in L can only be established by the action of torques due to wall stresses – again a demonstration of the role played by the solid domain boundaries.

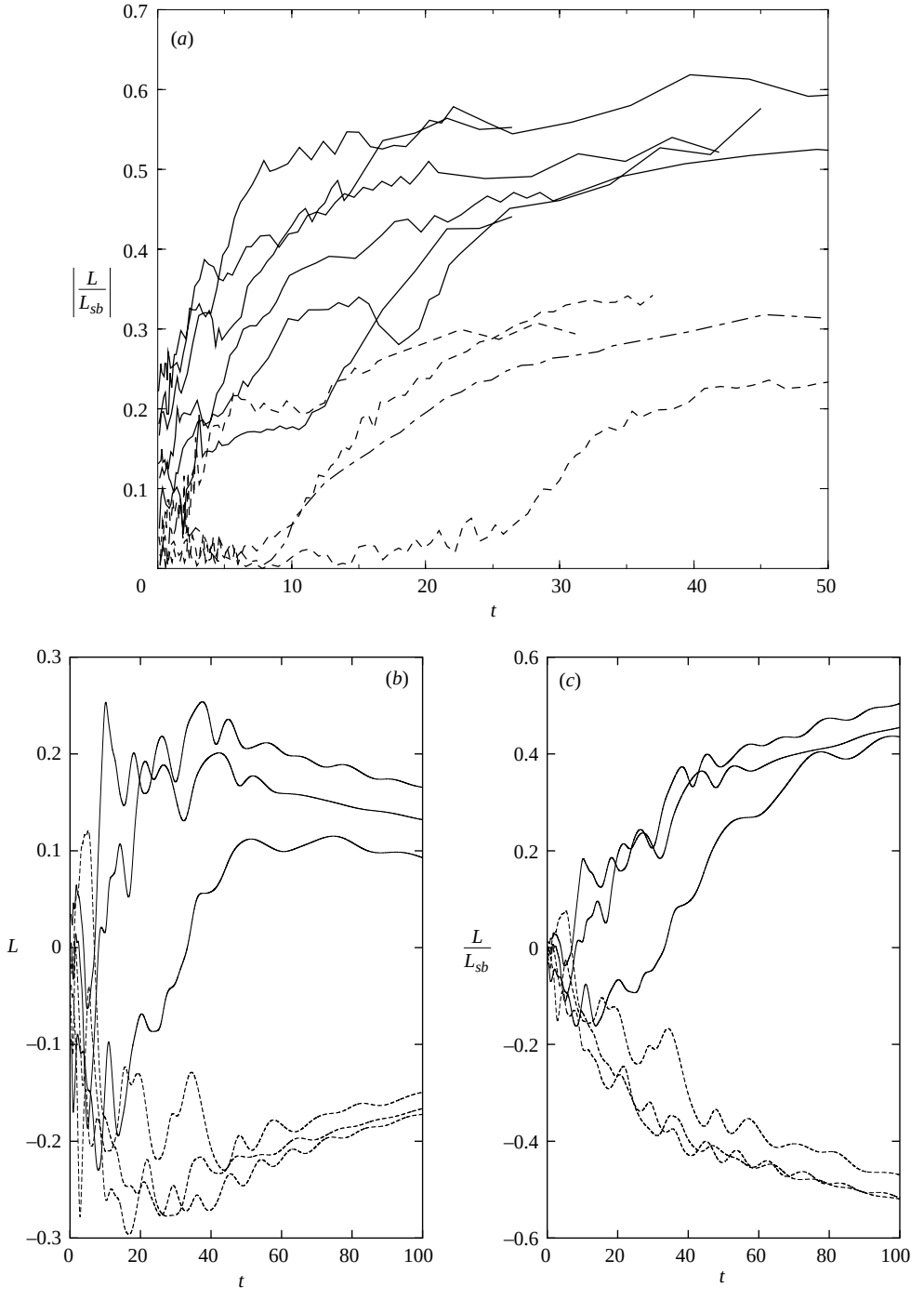

FIGURE 6. (*a*) Graphical representation of the normalized net angular momentum $L(t)/L_{sb}(t)$ found in a number of experiments – including the one shown in figure 3 – of decaying two-dimensional turbulence. The initial states are characterized by $L_0 \approx 0$ (dashed and dashed-dotted lines) and $|L_0| > 0$ (solid lines). The Reynolds number in these experiments is $Re^* = 5000$ (and $Re \approx 0.4Re^* = 2000$) (courtesy of S.R. Maassen 2000). (*b*) The angular momentum $L(t)$ for six runs from numerical simulations with $Re = 2000$, and (*c*) the normalized angular momentum $L(t)/L_{sb}(t)$ for these runs.

Laboratory experiments in which an initial non-zero angular momentum L_0 was introduced by forcing with an asymmetric grid show an approximately similar flow evolution, although the 'final state' of one large cell in the centre of the domain was reached more rapidly than in cases with $L_0 \approx 0$. Evidence is provided in figure 6(*a*) where the rapid spin-up is clearly visible for the runs with $L_0 \neq 0$. This behaviour is also observed in the evolution of the total angular momentum, which shows a much more rapid increase compared to the cases with $L_0 \approx 0$. These observations are confirmed by the spectral flow simulations.

4. Forced turbulence in a square no-slip domain

Direct numerical simulations of forced two-dimensional turbulence in a square domain with no-slip boundaries have been conducted. The scaling exponents (obtained from vorticity structure functions), (hyper) flatness and PDFs clearly indicate strong anisotropy of the turbulent flow and non-Gaussian statistics, as we will show below. In order to put this work in the right framework, we will briefly compare our results with those from either theoretical and numerical studies of two-dimensional unbounded turbulence (where boundary effects are absent) or with some experimental data (where perfect two-dimensionality is absent) to highlight the different conclusions from the various approaches. In our view the results from the various set-ups are not contradictory as such because different systems are considered. We should emphasize that boundedness and the kind of boundary conditions may result in different observations as anticipated from previous numerical studies on two-dimensional turbulence and experiments on quasi-two-dimensional turbulent flows.

It was shown by Molenaar, Clercx & van Heijst (2004) that spin-up-like phenomena may also be observed if a time-dependent forcing $q(t, \boldsymbol{x})$ is applied to the vorticity equation, generating a two-dimensional fluid flow from a set of zero initial conditions, $\omega_0(\boldsymbol{x}) = 0$. The stochastic forcing protocol is a first-order Markov chain, introduced by Lilly (1969) and described in some detail by Maltrud & Vallis (1991). In discrete-time notation, the first-order Markov chain with correlation coefficient r and amplitude A_0, applied to wavevector $\boldsymbol{k}$ is

$$q(n, \boldsymbol{k}) = rq(n-1, \boldsymbol{k}) + \left(1 - r^2\right)^{1/2} A_0 \mathrm{e}^{\mathrm{i}\pi\psi(n,\boldsymbol{k})}, \tag{4.1}$$

where the random variable $\psi(n, \boldsymbol{k})$ is drawn from a Gaussian distribution. The Markov chain is applied to a shell of wavenumbers $|\boldsymbol{k}| \in [7, 9]$ with $A_0 = 6.0$ and $r = 0.98$, see Molenaar *et al.* (2004) for details, and can be compared to a mechanical stirring device, moving slowly through the fluid in a random order. The computational resolution equals 161 or 257 nodes in each spatial direction, with a corresponding time steps $\delta t = 3.4 \times 10^{-4}$ and 1.35×10^{-4}, respectively.

The integral-scale Reynolds number, denoted as Re^*, is based on the time- and domain-averaged (root-mean-square) velocity scale

$$U \equiv \langle \sqrt{2E(t)} \rangle, \tag{4.2}$$

achieving a value on the order of $Re^* \simeq 3000$. As in the case of decaying flow, for these stochastically forced flows, the phenomenology is dominated by the generation of a large circulation cell, occupying most of the interior of the domain. However, in contrast to the decaying case, in the forced flow several consecutive events of rapid build-up and collapse of the circulation cell occur, where a spontaneous sign reversal of the angular momentum of the flow is possible from one event to the next. Such a sequence of events is shown in figure 7, in three consecutive snapshots of

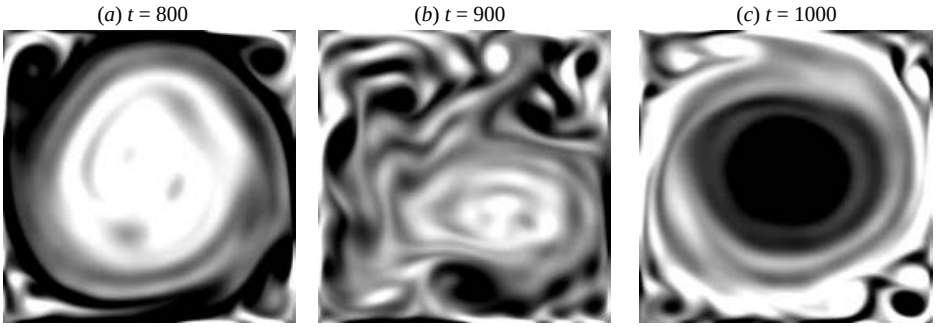

FIGURE 7. Snapshots of the vorticity evolution during the sign reversal of a large monopolar vortex structure for $Re \simeq 3000$, with vorticity levels ranging from $\omega < -5$ (black) to $\omega > 5$ (white).

the vorticity field, depicting a breakdown and a subsequent build-up, with opposite sign, of a large coherent structure. These observations above seem to complement the experimental results by Paret & Tabeling (1998), in which a large circulation cell dominated the flow in electromagnetically driven thin fluid layer experiments (where the flow dynamics is, however, strongly influenced by bottom friction). The phenomenon of formation and subsequent breakdown of larger cells was observed earlier by Sommeria (1986) in a laboratory experiment on steadily forced flows in a thin layer of mercury, under the influence of viscosity. Owing to the very limited experimental resolution, the mechanism explaining the large-scale reversals remained unclear. Numerical simulations of two-dimensional turbulence with bottom friction in a bounded domain with stress-free lateral boundaries ($\omega = 0$ on $\partial\mathscr{D}$), were performed by Verron & Sommeria (1987). These simulations support the experiments but, obviously, boundary layers near the lateral walls, that might destabilize the large central vortex, are absent in these simulations.

There seems to be an analogy with convection systems as the spontaneous sign-reversals of a large circulation cell are similar to the spontaneous sign-reversals of a feature known as 'the wind' in confined thermal convection, described by Niemela *et al.* (2001), see also the review article by Kadanoff (2000). However, while these authors speculated upon the cause of the observed large-scale instabilities, the definite cause was not established†, while our computations suggest that the viscous boundary layers may play a crucial role in these issues. Each collapse of the circulation cell is caused by the destabilizing effect of intense boundary layers and is associated with a decrease in the value of the absolute angular momentum. Consequently, the evolution of other relevant integral quantities, such as the energy $E(t)$ and the enstrophy $Z(t)$, is strongly influenced by the spin-up events.

Time series of these latter quantities during a $Re^* \simeq 3000$ computation, normalized by their respective mean values, are shown in figure 8. In the energy time series the spin-up effect is clearly recognizable in the form of clear peaks, reaching up to three

† An interesting theoretical analysis of the abrupt and irregular reversals of the large-scale circulation in turbulent Rayleigh–Bénard convection was put forward recently by Fontenele Araujo, Grossmann & Lohse (2004). It is based on the force and thermal balance on a single plume parcel. From the resulting nonlinear equations, related to the Lorenz equations, a phase diagram in the plane set up by the Prandtl and Rayleigh numbers can be constructed showing transitions to a regime of chaotic wind reversals.

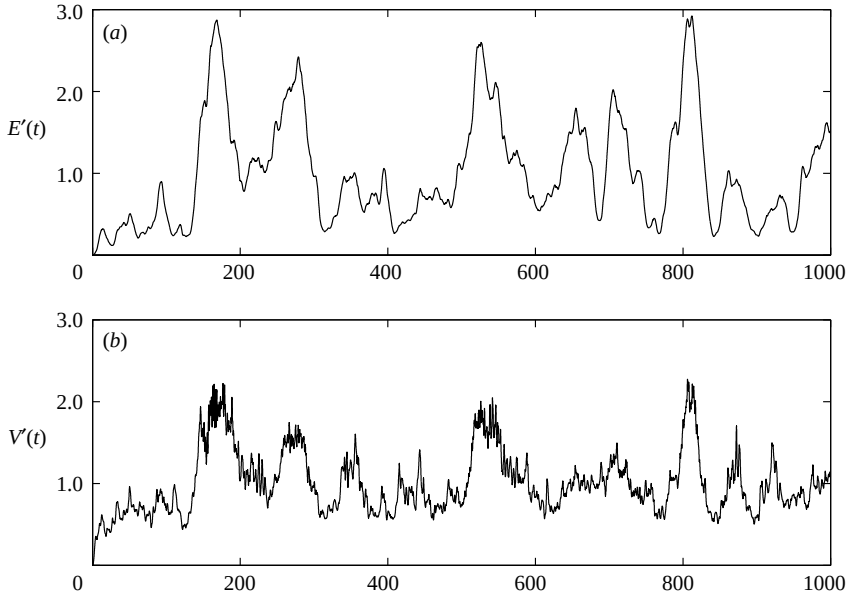

FIGURE 8. Evolution of the normalized energy, $E'(t)$, and enstrophy, $V'(t)$.

times average values. These peaks correspond to a condensation of energy within the large circulation cell, as was conjectured by Kraichnan (1967).

The evolution of the enstrophy is directly influenced by the formation of viscous boundary layers at the no-slip walls. These boundary layers are sources of opposite-signed vorticity, as compared to the central cell. Hence, these structures are sources of enstrophy $V(t)$, which is proportional to the destruction term in the global energy balance,

$$\frac{\mathrm{d}E(t)}{\mathrm{d}t} = -\frac{2}{Re}V(t) + \int_{\mathscr{D}} \boldsymbol{f}\cdot\boldsymbol{u}\,\mathrm{d}A, \tag{4.3}$$

where the inner product term on the right-hand side represents the energy input due to the forcing. Note that the simulation results of figures 7 and 8 are shown in dimensionless simulation time units. One could reformulate time in terms of a turnover time of the largest eddies, T_e, which is defined by means of the maximum measured root-mean-square velocity and the half-width of the domain, W,

$$T_e = \frac{W}{\max\limits_t \sqrt{2E(t)}}. \tag{4.4}$$

In such a formulation, the computations shown in figure 8 run up to $300T_e$.

The global phenomenological picture is in sharp contrast with observations of forced two-dimensional turbulence on a double-periodic domain. There the usual end state is a domain-filling dipole structure, which was first observed in direct numerical simulations by Hossain, Matthaeus & Montgomery (1983) and later by Smith & Yakhot (1993, 1994). Strong deviations from the double-periodic setting, due to the presence of boundary layers, had already been observed by Li & Montgomery (1996) and Li *et al.* (1996, 1997), in the case of decaying flow in a circular no-slip domain. These authors noted the change in early-time dissipative properties of the flow, under the action of boundary-layer development. In this respect, our observations highlight

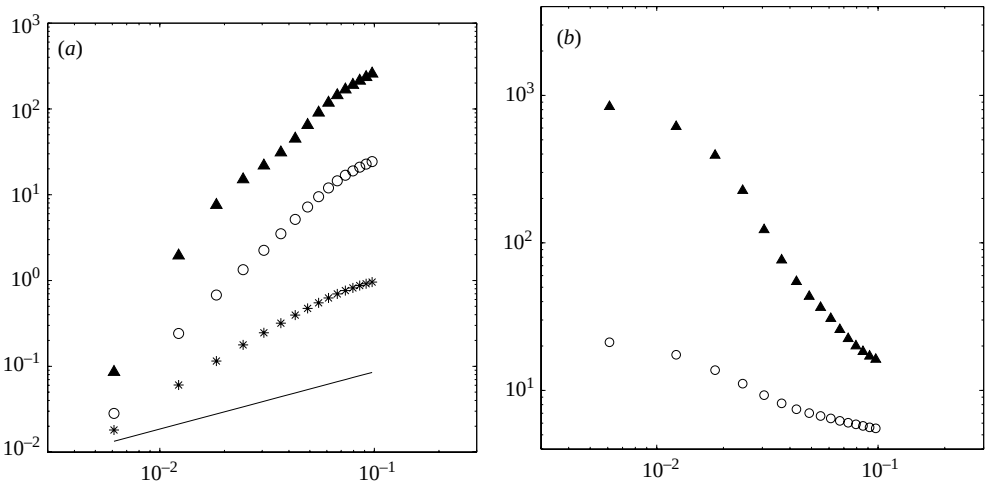

FIGURE 9. (*a*) Double logarithmic plot of normalized vorticity structure functions, of order $n = 2$ (stars), $n = 4$ (circles) and $n = 6$ (triangles) versus separation length $|\boldsymbol{r}|$, where the solid line corresponds to $\zeta(n) = 2/3$. (*b*) Double logarithmic plot of flatness (circles) and hyperflatness of (*b*) order $n = 3$ (filled triangles) against separation length.

a sharp difference with continuously forced flows in a double-periodic domain, where often some kind of additional energy dissipation is applied to achieve a stationary energy balance, such as e.g. the Ekman damping applied by Maltrud & Vallis (1991) or the hypo-viscosity operator applied by Borue (1993), where an inverse dissipation operator is added to the equations of motion with $\nu\Delta^{-p}$, for $p = 4, 6, 8, \ldots$. For the forced, wall-bounded flows considered here, it is found that the no-slip walls provide a natural energy dissipation mechanism, by means of the generation of viscous boundary layers.

The dramatically different phenomenology of the forced flows on a square no-slip domain, as opposed to the square double-periodic domain is also likely to have a pronounced influence on the corresponding scaling behaviour. Especially, the vorticity statistics are thought to deviate, since small-scale filaments, in the form of detached viscous boundary layers, play such an important role in the dynamics. The most important statistical tool used to analyse the flow is based on spatial vorticity differences, taken over the length scale $r = |\boldsymbol{r}|$,

$$\delta\omega(\boldsymbol{r}) = \omega(\boldsymbol{x} + \boldsymbol{r}) - \omega(\boldsymbol{x}). \tag{4.5}$$

Raising the differences to the power n followed by ensemble averaging $\langle\cdot\rangle$, yields the nth-order vorticity structure function

$$S_n(\omega(\boldsymbol{r})) = \langle(\delta\omega(\boldsymbol{r}))^n\rangle, \tag{4.6}$$

which is assumed to show a scaling behaviour with the separation length, as a function of order n,

$$S_n(\omega(\boldsymbol{r})) \sim r^{\zeta(n)}. \tag{4.7}$$

According to the classical theory of two-dimensional turbulence, the isotropic situation should yield zero scaling exponents for the vorticity structure functions of all orders.

Vorticity structure functions of orders 2, 4 and 6 are plotted against separation length in a double logarithmic graph in figure 9(*a*). The convergence of the statistics has been checked with the method of Belin, Tabeling & Willaime (1996) and it was

n	2	4	6
$\zeta(n)$	1.3 ± 0.1	2.2 ± 0.1	2.7 ± 0.2

TABLE 1. Scaling exponents for the structure functions of order n.

proved by Molenaar (2004) to be sufficient for the vorticity structure functions of orders up to 6 (note that record lengths are $O(10^6)$ points). Clearly, our results show non-zero scaling exponents for the wall-bounded, purely two-dimensional setting, with the value of the exponents listed in table 1.

The measurements of vorticity increments are taken in the centre of the domain, throughout a small square $B(r)$ of side r. In such a manner one might reduce the influence of the boundaries and achieve a more or less isotropic situation. It was argued by Paret, Jullien & Tabeling (1999) that experiments in a quasi-two-dimensional flow in a square cell yielded isotropic results for the vorticity statistics, after sufficient record lengths were averaged. These authors observed zero scaling exponents for the vorticity structure functions up to order 10.

The solid line in figure 9(a) shows $\zeta(n) = 2/3$, corresponding to the upper bound on the scaling exponents of vorticity structure functions of any order in the isotropic situation, as derived by Eyink (1995). A basic assumption for Eyinks' estimate was a constant enstrophy flux. Clearly, our observations for the second-order structure function exponent exceed 2/3, but are not as steep as the prediction $\zeta(2) > 2$, again for the isotropic situation, by Tran & Bowman (2002). An explanation for the deviations from both the Eyink model and the Tran & Bowman prediction may be found in both the non-constant enstrophy flux on a bounded domain, due to the generation of vorticity in the viscous boundary layers, and the anisotropy of the flow.

To test for Gaussianity in the scaling results, figure 9(b) shows the flatness and hyperflatness of order $n = 3$, corresponding to the data in figure 9(a). These quantities are respectively defined as

$$F(\boldsymbol{r}) := \frac{S_4(\omega(\boldsymbol{r}))}{(S_2(\omega(\boldsymbol{r})))^2} \quad \text{and} \quad H_{2n}(\boldsymbol{r}) := \frac{S_{2n}(\omega(\boldsymbol{r}))}{(S_2(\omega(\boldsymbol{r})))^n} \quad \text{for} \quad n = 3. \tag{4.8}$$

If $H_{2n}(\boldsymbol{r})$ is independent of separation length r, no intermittency is present, which, by the multi-fractal scaling model, results in scaling exponents $\zeta(2n) = n\zeta(2)$ or $\zeta(n) \propto n$.

The corresponding Gaussian values are 3 and 15 for the flatness and third-order hyperflatness, respectively, from which the computational data deviate strongly, moving towards smaller scales. On the other hand, both the results for the (hyper) flatness and the scaling exponents of the vorticity structure functions may be different for higher integral-scale Reynolds numbers, where the behaviour is different. At present higher integral-scale Reynolds numbers are not attainable computationally owing to the necessary long-time statistical averaging. Currently, new computational techniques are being developed for this purpose.

Finally, we compare the normalized probability distribution function (PDF) of vorticity increments in the wall region with that measured in the interior of the domain. In the preceding paragraphs we deliberately took measurements of vorticity increments at some distance from the domain boundary, to avoid obvious bias expected to occur near the wall. For three-dimensional turbulence Benzi *et al.* (1999) compared small-scale velocity statistics measured near a no-slip wall with statistics

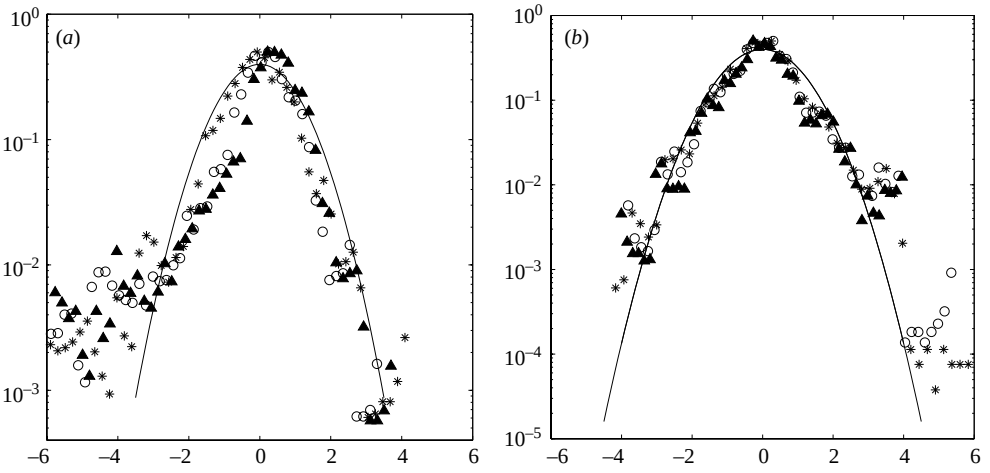

FIGURE 10. Log-linear plot of the PDF, $P(s')$, of normalized vorticity increments, $s'(\boldsymbol{r})$, with $r = 0.006$ (stars), $r = 0.012$ (circles) and $r = 0.024$ (filled triangles), where the solid line represents a Gaussian normal PDF, (*a*) near the wall and (*b*) in the interior of the domain. Measurements in (*a*) were taken in the wall-normal direction.

measured in the bulk of the flow, and they found an increase in deviations from Gaussian behaviour when moving towards the wall. In figure 10(*a*) we show the PDF of normalized vorticity increments in the wall region, measured in the normal-wall direction, at three separation lengths, and the corresponding PDF in the interior in figure 10(*b*). Clearly, deviations from the normal distribution, shown in the figure as solid lines, are very pronounced in the near-wall region, although smaller deviations also occur in the interior for separation lengths $r = 0.006$ and $r = 0.012$. In the wall region the deviations are still marked for $r = 0.024$, but this is not the case in the interior.

5. Discussion and conclusions

The type of boundary condition apparently plays an important role in the evolution of confined two-dimensional turbulence, both for the decaying and the continuously forced case. It has been found in laboratory experiments as well as numerical simulations of decaying two-dimensional turbulence in a square domain with no-slip walls that the quasi-stationary late-time state of the flow consists of a single domain-filling cell, surrounded by a band of opposite-signed vorticity. This final state, ultimately decaying towards the fundamental 'Stokes mode' in a square domain (see Van de Konijnenberg, Flór & van Heijst 1998), is in marked contrast with late-time behaviour observed for the cases of stress-free boundaries or double-periodicity: in the latter case the flow becomes organized into a pair of equal cells of opposite vorticity, while for stress-free walls one commonly observes organization into an asymmetric dipolar flow structure (Brands *et al.* 1999). Laboratory experiments – with initial motion ($Re^* \approx 5000$) generated by a translating grid – and high-resolution numerical simulations – initialized by a perturbed array of 10×10 vortices ($Re = 2000$) – have revealed the crucial role of the no-slip walls, namely as sources of high-amplitude vorticity filaments. These filamentary structures are advected away from the walls, and hence affect the flow evolution in the interior. A remarkable feature in the evolution is the so-called 'spontaneous spin-up', corresponding to the formation of

the domain-filling cell (which can be in either rotation sense). At this stage the total angular momentum L shows a rapid increase (even when starting with an initial state with $L_0 \approx 0$), thus revealing the role of the walls in providing forces (both normal and shear stresses) and torques that lead to a change in L. Experiments and numerical simulations have revealed that an initial non-zero angular momentum $|L_0| > 0$ promotes the spin-up significantly.

The remarkable role of no-slip walls is also observed in high-resolution simulations of continuously forced turbulence. In confined forced flows, the self-organizing tendency may be disrupted by the disorganizing 'stirring' introduced by a randomly arranged forcing: in the case of strong forcing the flow may never reach an organized state. On the other hand, when weakly forced the flow will become organized as a domain-filling cell, which is only slightly perturbed by the forcing applied. In § 4 we have shown simulation results for the intermediate case of moderate forcing, in which the no-slip sidewalls also play an important role in the flow evolution. In this forcing regime the flow becomes organized into a single large cell, which is subsequently destroyed due to lateral erosion by filamentary vorticity structures generated at the no-slip boundaries. After this state of disorder, the flow becomes organized again in a domain-filling cell with arbitrary rotation sense. Each time such a large cell is formed the total angular momentum L and kinetic energy E show a significant increase. A similar behaviour is seen in the evolution of the total enstrophy V, which is of course due to the enhanced formation of vorticity filaments at the solid walls. At the stage when the central cell is destroyed, both L, E and V show a rapid decrease. This repeated process of cell build-up and destruction is in marked contrast to the flow behaviour observed in forced two-dimensional turbulence on a double periodic domain (see e.g. Hossain *et al.* 1983; Smith & Yakhot 1993, 1994).

Because of the role of the no-slip walls as sources of high-amplitude vorticity filaments, it is not surprising that the scaling behaviour – in particular in the vorticity statistics – is also different compared to unconfined, isotropic two-dimensional turbulence. This behaviour has been examined by using the vorticity structure function S_n (of order n) and the associated flatness F and hyperflatness H_{2n}. The scaling exponents found in the numerical flow simulations for $Re^* \simeq 3000$ are remarkably different from those according to the classical theory of unbounded two-dimensional turbulence. The flatness and hyperflatness both appeared to deviate strongly for the corresponding Gaussian values. A similar deviation was found in the probability distribution function of vorticity increments, in particular when moving closer to the walls.

These observations reveal that the presence of no-slip boundaries affects the behaviour of two-dimensional turbulence (either continuously forced or decaying) in a rather dramatic way, their influence not being restricted to regions close to the perimeter but essentially extending over the full domain. Any comparison of laboratory experiments or numerical simulations of two-dimensional flows confined by no-slip walls with corresponding results for inviscid flow on doubly periodic domains requires caution.

The authors gratefully acknowledge financial support from the Dutch Foundation for Fundamental Research on Matter (FOM), which is financially supported by the Nederlandse Organisatie voor Wetenschappelijk Onderzoek (Netherlands Organization for Scientific Research, NWO). Part of this work was sponsored by the Stichting Nationale Computerfaciliteiten (National Computing Facilities Foundation, NCF) for the use of supercomputer facilities, with financial support from NWO.

REFERENCES

Belin, F., Tabeling, P. & Willaime, H. 1996 Exponents of structure functions in a low temperature helium experiment. *Physica* D **93**, 52–63.

Benzi, R., Amati, G., Casciola, C. M., Toschi, F. & Piva, R. 1999 Intermittency and scaling laws for wall bounded turbulence. *Phys. Fluids* **11**, 1284–1286.

Blevins, R. D. 1984 *Applied Fluid Dynamics Handbook*. Van Nostrand Reinhold.

Borue, V. 1993 Spectral exponents of enstrophy cascade in stationary two-dimensional homogeneous turbulence. *Phys. Rev. Lett.* **71**, 3967–3970.

Brands, H., Maassen, S. R. & Clercx, H. J. H. 1999 Statistical mechanical predictions and Navier-Stokes dynamics of two-dimensional flows on a bounded domain. *Phys. Rev.* E **60**, 2864–2874.

Chavanis, P. H. & Sommeria, J. 1996 Classification of self-organised vortices in two-dimensional turbulence: the case of a bounded domain. *J. Fluid Mech.* **314**, 267–297.

Clercx, H. J. H. 1997 A spectral solver for the Navier-Stokes equations in the velocity-vorticity formulation for flows with two non-periodic directions. *J. Comput. Phys.* **137**, 186–211.

Clercx, H. J. H. & van Heijst, G. J. F. 2000 Energy spectra for decaying two-dimensional turbulence in a bounded domain. *Phys. Rev. Lett.* **85**, 306–309.

Clercx, H. J. H. & van Heijst, G. J. F. 2002 Dissipation of kinetic energy in two-dimensional bounded flows. *Phys. Rev. E* **65**, 066305-1–4.

Clercx, H. J. H., Maassen, S. R. & van Heijst, G. J. F. 1998 Spontaneous spin-up during the decay of two-dimensional turbulence in a square container with rigid boundaries. *Phys. Rev. Lett.* **80**, 5129–5132.

Clercx, H. J. H., Maassen, S. R. & van Heijst, G. J. F. 1999 Decaying two-dimensional turbulence in square containers with no-slip or stress-free boundaries. *Phys. Fluids* **11**, 611–626.

Clercx, H. J. H., Nielsen, A. H., Torres, D. J. & Coutsias, E. A. 2001 Two-dimensional turbulence in square and circular domains with no-slip walls. *Eur. J. Mech.* B/*Fluids* **20**, 557–576.

Eyink, G. L. 1995 Exact results on scaling exponents in the two-dimensional enstrophy cascade. *Phys. Rev. Lett.* **74**, 3800–3803.

Fincham, A. M., Maxworthy, T. & Spedding, G. R. 1996 Energy dissipation and vortex structure in freely decaying, stratified grid turbulence. *Dyn. Atmos. Oceans* **23**, 155–169.

Fontenele Araujo, F., Grossmann, S. & Lohse, D. 2005 Wind reversals in turbulent Rayleigh-Bénard convection. *Phys. Rev. Lett.* **95**, 084502.

Hossain, M., Matthaeus, W. H. & Montgomery, D. 1983 Long-time state of inverse cascades in the presence of a maximum length scale. *J. Plasma Phys.* **30**, 479–493.

Joyce, G. & Montgomery, D. 1973 Negative temperature states for the two-dimensional guiding centre plasma. *J. Plasma Phys.* **10**, 107–121.

Kadanoff, L. P. 2000 Turbulent heat flows: structure and scaling. *Phys. Today* **54**, 34–39.

Kellay, H. & Goldburg, W. I. 2002 Two-dimensional turbulence: a review of some recent experiments. *Rep. Prog. Phys.* **65**, 845–894.

Kraichnan, R. H. 1967 Inertial ranges in two-dimensional turbulence. *Phys. Fluids* **10**, 1417–1423.

Kraichnan, R. H. & Montgomery, D. 1980 Two-dimensional turbulence. *Rep. Prog. Phys.* **43**, 547–619.

Li, S. & Montgomery, D. C. 1996 Decaying two-dimensional turbulence with rigid walls. *Phys. Lett. A* **21**, 281–291.

Li, S., Montgomery, D. & Jones, W. B. 1996 Inverse cascades of angular momentum. *J. Plasma Phys.* **56**, 615–639.

Li, S., Montgomery, D. C. & Jones, W. B. 1997 Two-dimensional turbulence with rigid circular walls. *Theor. Comput. Fluid Dyn.* **9**, 167–181.

Lilly, D. 1969 Numerical simulation of two-dimensional turbulence. *Phys. Fluids* **12**, II, 240–249.

Maassen, S. R. 2000 Self-organization of confined two-dimensional flows. PhD Thesis, Eindhoven University of Technology.

Maassen, S. R., Clercx, H. J. H. & van Heijst, G. J. F. 1999 Decaying quasi-two-dimensional turbulence in a stratified fluid with circular boundaries. *Europhys. Lett.* **46**, 339–345.

Maassen, S. R., Clercx, H. J. H. & van Heijst, G. J. F. 2002 Self-organization of quasi-two-dimensional turbulence in stratified fluids in square and circular containers. *Phys. Fluids* **14**, 2150–2169.

Maassen, S. R., Clercx, H. J. H. & van Heijst, G. J. F. 2003 Self-organization of quasi-two-dimensional turbulence in stratified fluids in rectangular containers. *J. Fluid. Mech.* **495**, 19–33.

Maltrud, M. E. & Vallis, G. K. 1991 Energy spectra and coherent structures in numerical simulations of two-dimensional and beta-plane turbulence. *J. Fluid Mech.* **228**, 321–342.

Matthaeus, W. H. & Montgomery, D. C. 1980 Selective decay hypothesis at high mechanical and magnetic Reynolds numbers. *Ann. (N.Y.) Acad. Sci.* **357**, 203–222.

Matthaeus, W. H., Stribling, W. T., Martinez, D., Oughton, S. & Montgomery, D. C. 1991 Decaying, two-dimensional, Navier-Stokes turbulence at very long times. *Physica* D **51**, 531–538.

McWilliams, J. C. 1984 The emergence of isolated coherent vortices in turbulent flows. *J. Fluid Mech.* **146**, 21–43.

Miller, J. 1990 Statistical mechanics of Euler's equation in two dimensions. *Phys. Rev. Lett.* **65**, 2137–2140.

Molenaar, D. 2004 Forced Navier-Stokes flows on a bounded two-dimensional domain. PhD Thesis, Eindhoven University of Technology.

Molenaar, D., Clercx, H. J. H. & van Heijst, G. J. F. 2004 Angular momentum of forced two-dimensional turbulence on a square no-slip domain. *Physica* D **196**, 329–340.

Niemela, J. J., Skrbek, L., Sreenivasan, K. R. & Donnelly, R. J. 2001 The wind in confined thermal convection. *J. Fluid Mech.* **449**, 169–178.

Onsager, L. 1949 Statistical hydrodynamics. *Nuovo Cimento Suppl.* **6**, 279–287.

Paret, J., Jullien, M. & Tabeling, P. 1999 Vorticity statistics in the two-dimensional enstrophy cascade. *Phys. Rev. Lett.* **83**, 3418–3421.

Paret, J. & Tabeling, P. 1998 Intermittency in the two-dimensional inverse cascade of energy: Experimental observations. *Phys. Fluids* **10**, 3126–3136.

Pointin, Y. B. & Lundgren, T. S. 1976 Statistical mechanics of two-dimensional vortices in a bounded container. *Phys. Fluids* **19**, 1459–1470.

Robert, R. 1991 Maximum entropy principle for two-dimensional Euler equations. *J. Stat. Phys.* **65**, 531–553.

Santangelo, P., Benzi, R. & Legras, B. 1989 The generation of vortices in high-resolution two-dimensional, decaying turbulence and the influence of initial conditions on the breaking of self-similarity. *Phys. Fluids* A **1**, 1027–1034.

Smith, L. M. & Yakhot, V. 1993 Bose condensation and small-scale structure generation in a random force driven two-dimensional turbulence. *Phys. Rev. Lett.* **71**, 352–355.

Smith, L. M. & Yakhot, V. 1994 Finite-size effects in forced two-dimensional turbulence. *J. Fluid Mech.* **274**, 115–138.

Sommeria, J. 1986 Experimental study of the two-dimensional inverse energy cascade in a square box. *J. Fluid Mech.* **170**, 139–168.

Tabeling, P. 2002 Two-dimensional turbulence: a physicist approach. *Phys. Rep.* **362**, 1–62.

Tran, C. V. & Bowman, J. C. 2002 On the dual cascade in two-dimensional turbulence. *Physica* D **176**, 242–255.

Van de Konijnenberg, J. A., Flór, J. B. & van Heijst, G. J. F. 1998 Decaying quasi-two-dimensional flow on a square domain. *Phys. Fluids* **10**, 595–606.

Verron, J. & Sommeria, J. 1987 Numerical simulations of a two-dimensional turbulence experiment in magnetohydrodynamics. *Phys. Fluids* **30**, 732–739.